surfaces

MDPI

Article

Thin-Film Formation from Lactic Acid via Open-Air Plasma Polymerization

Sho Yoshida, Taiki Osawa, Masaya Tahara, Akito Shirai, Hua-Ting Hsieh, Taisei Fukawa, Akane Yaida and Akitoshi Okino *

Laboratory for Future Interdisciplinary Research of Science and Technology, Institute of Science Tokyo, J2-32, 4259 Nagatsuta, Midori-ku, Yokohama 226-8501, Japan; yoshida.s.29ba@m.isct.ac.jp (S.Y.); osawa.t.0e00@m.isct.ac.jp (T.O.); tahara.m.e921@m.isct.ac.jp (M.T.); shirai.a.d385@m.isct.ac.jp (A.S.); hsieh.h.7044@m.isct.ac.jp (H.-T.H.); fukawa.t.c455@m.isct.ac.jp (T.F.); yaida@first.iir.isct.ac.jp (A.Y.)
* Correspondence: aokino@first.iir.isct.ac.jp; Tel.: +81-45-924-5688

Abstract

This study investigates the formation mechanism of lactic-acid-derived coatings produced by open-air atmospheric-pressure plasma polymerization. A comparison of nebulization and bubbling precursor-delivery methods using FT-IR and XPS showed that the bubbling method facilitated plasma-assisted chemical bonding, including the possible formation of copper(II) lactate-like interfacial species and the retention of carbonyl-containing functional groups. However, the present dataset does not provide direct, discriminating evidence for a specific metal-lactate interfacial species, and alternative interpretations such as adsorption, oxidation, hydroxylation, or generic oxygenated carbon deposition cannot be excluded. Time-dependent analysis revealed a transition from oxygen-rich functional layers at short plasma exposure to carbon-rich overlayers at longer exposure, suggesting a fragmentation-recombination mechanism that is consistent with the formation of a metal-lactate-like interfacial region and a carbon-rich overlayer, while alternative interpretations related to signal attenuation and non-uniform coverage remain possible. Antibacterial testing revealed that the observed bacterial responses were not attributable to an intrinsic antibacterial property of the deposited films, but were instead strongly dependent on the underlying substrate chemistry and exposure time. C1100 retained the inherent antibacterial activity of copper, SUS430 showed no activity due to the absence of film formation, and SPCC exhibited only a transient effect attributed to lactic-acid-induced local acidification. Overall, the study elucidates the plasma-assisted deposition mechanism of lactic-acid-derived coatings under open-air conditions and highlights the critical role of interface chemistry in achieving stable and substrate-independent functional properties.

Keywords: atmospheric pressure plasma polymerization; lactic acid; surface modification; open-air plasma

Check for updates

Academic Editors: Aleksey Yerokhin and Maurice Brogly

Received: 24 December 2025
Revised: 3 March 2026
Accepted: 16 March 2026
Published: 29 March 2026

Copyright: © 2026 by the authors. Licensee MDPI, Basel, Switzerland. This article is an open access article distributed under the terms and conditions of the Creative Commons Attribution (CC BY) license.

1. Introduction

In recent years, surface treatment technologies have evolved as indispensable foundational techniques across diverse industrial sectors. Among these, the development of functional surfaces—such as those with enhanced adhesion and antibacterial properties—has attracted considerable attention for improving safety in medical, food, and living environments, as well as for contributing to the realization of a sustainable society. Traditionally, surface modification of metals and polymeric materials has relied on thermal,

chemical, and physical treatments. However, plasma-based surface treatment technologies have rapidly advanced as an approach that simultaneously achieves reduced environmental impact and enhanced functionality [1–3].

Plasma treatment offers significant advantages, including substantial surface modification effects with minimal penetration depth, thereby preserving bulk properties. Furthermore, as a dry process, it imposes a low environmental burden. The development of atmospheric-pressure low-temperature plasma has enabled minimal thermal influence on substrates and continuous processing, contributing to reduced implementation and maintenance costs and improved productivity in industrial applications [4–8]. Moreover, Chemical Vapor Deposition (CVD), which was previously feasible only under vacuum conditions, can now be performed in open systems, opening new possibilities for continuous product processing and even biomedical applications [9]. In this context, plasma-assisted film formation has evolved to include open-air atmospheric-pressure plasma polymerization, in which organic precursors are fragmented and recombined into highly cross-linked polymer-like thin films.

The formation of high-performance films via open-air plasma polymerization offers diverse functionalities—such as adhesion, antibacterial activity, and conductivity—through appropriate precursor selection, while minimizing adverse effects on substrate properties. Nevertheless, most reported studies have been limited to closed systems, and research on film formation using high-molecular-weight or antibacterial monomers under open-air plasma polymerization conditions remains extremely limited [10].

The development of antibacterial materials has become increasingly important in medical and food sectors from the perspectives of infection control and hygiene management. In particular, coating technologies employing biocompatible antibacterial monomers—such as lactic acid, citric acid, linseed oil, and medium-chain triglyceride (MCT) oil—are expected to provide a novel approach that combines environmental sustainability with safety. However, reports on open-air plasma polymerization processes using these monomers are scarce, and the mechanisms underlying film formation and antibacterial functionality remain largely unexplored.

In this study, we applied a precursor delivery system to a linear-type atmospheric-pressure plasma device equipped with a gas-flow control mechanism and radio-frequency discharge [11,12] to investigate the formation mechanism and surface chemistry of lactic-acid-derived films prepared by open-air plasma polymerization, and to critically evaluate their antibacterial responses in relation to substrate effects. Specifically, we focused on lactic acid as a precursor and compared bubbling and nebulization methods for precursor supply, while evaluating film deposition behavior, chemical bonding states, and surface morphology on metallic substrates. Furthermore, comprehensive analyses using X-ray Photoelectron Spectroscopy (XPS), Fourier Transform Infrared Spectroscopy (FT-IR), and Scanning Electron Microscopy (SEM) were conducted to elucidate molecular structural changes induced by plasma treatment and self-assembly phenomena. We further included antibacterial testing as a secondary functional check to determine whether any coating-attributable effect could be distinguished from substrate-driven or transient effects.

2. Materials and Methods

2.1. Plasma Generation System and Experimental Configuration

Plasma generation was performed using a custom-developed linear-type atmospheric-pressure plasma device based on the dielectric barrier discharge (DBD) method. This system enables continuous processing under open-air conditions and can generate plasma over a maximum width of 349 mm, allowing substrate conveyance and large-area treatment.

To implement the open-air plasma polymerization process, a precursor delivery unit was integrated into the system. The overall configuration of the apparatus is shown in Figure 1.

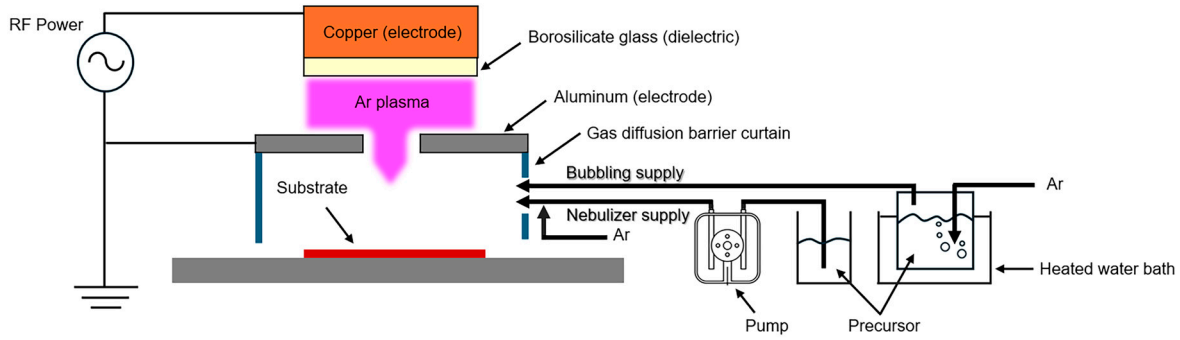


Figure 1. Schematic representation of the open-air plasma polymerization apparatus.

Argon gas was employed as the plasma-generating medium at a flow rate of 30 L/min. The radio-frequency power supply (PRF-125C, ANELVA/Canon Anelva Corporation, Kanagawa, Japan) operated at 13.56 MHz with an applied power of 200 W. Precursors were introduced using either a bubbling system or a nebulizer. In the bubbling method, the precursor was heated in a water bath to control vapor supply, with the heating temperature set at 60 °C. The distance between the plasma and the substrate was maintained at 30 mm. To minimize the diffusion of precursor mist or vapor, a diffusion-prevention curtain was installed around the plasma region.

2.2. Chemical Precursors and Substrate Materials

The following precursors were selected for antibacterial coating formation: lactic acid (FUJIFILM Wako Pure Chemical Corporation, Osaka, Japan), medium-chain triglyceride (MCT) oil (Nisshin OilliO Group, Ltd., Tokyo, Japan), linseed oil (Nisshin OilliO Group, Ltd., Tokyo, Japan), and citric acid (Kenei Pharmaceutical Co., Ltd., Osaka, Japan). The CAS number of lactic acid is 50-21-5. MCT oil is a mixture primarily composed of octanoic acid (CAS No. 124-07-2, 60%) and decanoic acid (CAS No. 334-48-5, 20%). Linseed oil (CAS No. 8001-26-1) mainly contains α-linolenic acid (CAS No. 463-40-1, 56%) and oleic acid (CAS No. 112-80-1, 19%). Citric acid (CAS No. 5949-29-1) was dissolved in methanol (FUJIFILM Wako Pure Chemical Corporation, Osaka, Japan) to prepare a 20 wt% methanol solution. The CAS number of methanol is 67-56-1. These precursors have been reported to exhibit antibacterial properties [13–16].

For film deposition, plate-type substrates of C1100 copper, SUS430 stainless steel, and SPCC cold-rolled steel with dimensions of 15 × 15 mm and a thickness of 0.5 mm were used. C1100 (purity ≥ 99.94%) was purchased from Kenis Co., Ltd. (Osaka, Japan), SUS430 from Hikari Co., Ltd. (Osaka, Japan), and SPCC from Taiho Trading Co., Ltd. (Tokyo, Japan). Prior to coating, all metal substrates were ultrasonically cleaned in acetone for 5 min to remove organic contaminants.

As a comparative material, borosilicate cover glass (thickness: 0.12–0.17 mm, size: 18 × 18 mm) manufactured by Matsunami Glass Ind., Ltd. (Osaka, Japan) was used. The cover glass was sterilized by autoclaving at 121 °C for 20 min before use.

C1100 (copper) and SPCC (cold-rolled steel) were selected as models of metals prone to oxidation [17–19], whereas SUS430 (stainless steel) was chosen as a representative metal characterized by passivation through chromium oxide film formation [20]. Copper exhibits excellent antibacterial properties [21,22], and its combination with lactic acid or linseed oil allows evaluation of potential synergistic effects. Furthermore, copper's superior electrical and thermal conductivity makes it highly applicable to medical devices and

food processing equipment. SPCC is a widely used, low-cost steel material for industrial applications; if antibacterial performance can be enhanced through coating, it would represent a promising technology for cost-effective antibacterial functionality. SUS430 offers excellent corrosion resistance and is commonly employed in food and medical sectors; assessing the antibacterial potential of lactic acid coatings on SUS430 provides insights into practical applicability.

The use of MCT oil, linseed oil, and citric acid in this study was limited to preliminary screening for evaluating biocompatible candidate precursors. Detailed optimization and mechanistic analysis of these materials were beyond the primary scope of the present work.

2.3. Precursor Delivery Method and Plasma Deposition Parameters

To activate the precursor within the plasma, mist or vapor was introduced into the argon plasma generated 30 mm above the substrate surface. Comparative experiments were conducted using both nebulization and bubbling methods, with and without plasma irradiation, to evaluate changes in the substrate surface after treatment.

In the bubbling method, argon gas was passed through the precursor liquid at a flow rate of 5 L/min, supplying vapor as the carrier gas. For citric acid, which was prepared as a solid-methanol mixture, only the nebulization method was applied. The nebulizer used was model G8010-60270 (Agilent Technologies Inc., Santa Clara, CA, USA), and the pump was RP-PJ AC type (Sanyo Technos Co., Ltd., Saitama, Japan). Argon gas was supplied at 1 L/min, and the precursor was delivered as mist with a particle size of several micrometers at a flow rate of 30 mL/min.

2.4. Estimation of Molecular Flux and Surface Coverage in Bubbling Method

The number of molecules of lactic acid, MCT oil, and linseed oil was calculated according to the procedure described in [23]. First, the vapor pressure at 60 °C (333 K) was determined using the Clausius-Clapeyron equation, where the reference temperature was set to the boiling point of each substance and the reference vapor pressure (P_{ref}) was assumed to be 1 atm [24–27].

$$ln\frac{P}{P_{ref}} = -\frac{\Delta H_{vap}}{R}\left(\frac{1}{T} - \frac{1}{T_{ref}}\right)$$

Here, P represents the vapor pressure at the target temperature (Pa), R is the gas constant (8.314 J·mol^{-1}·K^{-1}), T is the target temperature (K), and T_{ref} is the reference temperature (K).

$$n = \frac{P}{RT}$$

Next, the number of moles contained in 1 m^3 of air was calculated using the ideal gas law, and finally converted to the number of molecules using Avogadro's constant ($N_A = 6.022 \times 10^{23}$ mol^{-1}).

$$N = n \times N_A \quad (1)$$

For MCT oil, the representative value was determined by averaging the boiling points and enthalpies of vaporization of tricaprylin (C8) and tricaprin (C10), whereas for linseed oil, the calculation was based on α-linolenic acid.

The calculation results are summarized in Table 1. Lactic acid exhibited relatively high vapor pressure; when supplied for 30 s at an argon flow rate of 5 L/min using the bubbling method, the number of molecules contained in the argon gas was approximately 1.96×10^{20}. In contrast, the number of molecules of MCT oil and linseed oil were approximately

3.78×10^{16} and 8.70×10^{11}, respectively, which are significantly lower than that of lactic acid but considered sufficient for film formation.

Table 1. Approximate vapor pressure and molecular number density of lactic acid, MCT oil, and linseed oil (estimated at 60 °C).

Precursor	Vapor Pressure (Pa) at 60 °C	Molecular Number Density (Molecules/m^3) at 60 °C
Lactic acid	3.59×10^{2}	7.82×10^{22}
MCT oil	6.94×10^{-2}	1.51×10^{19}
Linseed oil	1.60×10^{-4}	3.48×10^{14}

2.5. Characterization Techniques and Data Analysis

Surface chemical composition and bonding states were analyzed using XPS (ESCA1700R, ULVAC-PHI, Inc., Kanagawa, Japan) with a monochromatic Al Kα source (1486.6 eV, 245 W). High-resolution spectra were acquired at a pass energy of 23.5 eV with charge compensation. Binding energies were charge-referenced to the C 1s peak at 284.8 eV. For visualization of chemical-state changes (e.g., peak shapes and satellite features), the spectra were normalized to the maximum intensity of the C 1s peak. XPS spectra were processed using MultiPak software (ULVAC-PHI, Inc., Kanagawa, Japan). A Shirley-type background subtraction was applied. Importantly, no smoothing or averaging was applied to any of the displayed XPS spectra to avoid distortion of subtle spectral features (e.g., satellites/shoulders in Cu 2p). High-resolution scans were collected using an energy step of 0.05 eV and a dwell time of 40 ms per step. The acquisition windows were 280–295 eV for C 1s (3 sweeps) and 920–970 eV for Cu 2p (10 sweeps). To retain intensity information relevant to substrate signal attenuation and overlayer build-up, the time-dependent spectra are presented on a counts-per-second (c/s) scale without C 1s normalization. Because intensities are displayed as c/s (time-normalized), within-core-level intensity changes with treatment time are discussed as semi-quantitative trends. Semi-quantitative Cu 2p metrics calculated from these time-normalized spectra are reported in the Supplementary Information.

Molecular structure and functional groups of the deposited films were characterized by FT-IR (IRAffinity-1S, Shimadzu Corporation, Kyoto, Japan) in attenuated total reflectance (ATR) mode using an ATR accessory (QATR 10, Shimadzu Corporation, Kyoto, Japan). Spectra were recorded over the range of 4000–400 cm^{-1} with a resolution of 4 cm^{-1}, and 45 scans were averaged for each measurement. FT-IR spectral data were analyzed using LabSolutions IR software (ver. 2.30, Shimadzu Corporation, Kyoto, Japan). ATR correction was applied to account for wavelength-dependent penetration depth, and atmospheric correction was performed to remove contributions from ambient water vapor and carbon dioxide. To improve the signal-to-noise ratio, a 20-point moving average smoothing was applied. For comparison between samples, the spectra were normalised to the maximum absorbance intensity. No further spectral manipulation was conducted. Normalized spectra are presented to facilitate comparison of spectral features; however, normalization removes absolute-intensity information related to areal coverage and thickness.

Surface morphology and film thickness were examined using Scanning Electron Microscopy (SEM; JSM-IT100, JEOL Ltd., Tokyo, Japan). Samples were sputter-coated with a thin layer of gold prior to observation to prevent charging. SEM images were acquired at an accelerating voltage of 10 kV under high-vacuum conditions. SEM images were cropped to remove unused margins, but no smoothing, filtering, or morphological modifications were applied. Only uniform brightness and contrast adjustments were made using the instrument software (JEOL Ltd., Tokyo, Japan).

The antibacterial performance was assessed by measuring the residual bacterial count of *Escherichia coli* (ATCC 25922) to confirm the effectiveness against Gram-negative bacteria. The experimental procedure is illustrated in Figure 2. A 10 µL aliquot of *E. coli* suspension was dropped onto the coated substrates, and contact times of 2, 6, and 24 h were set. The evaluation was conducted in accordance with ISO 22196 [28], with additional short-time assessments to account for the inherent antibacterial activity of copper [29,30]. Contact between the bacteria and the substrate was maintained at 20 °C and 30% relative humidity.

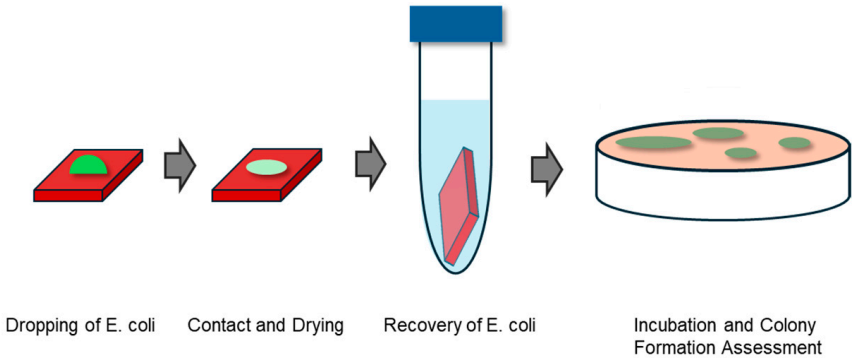


Figure 2. Schematic representation of the antibacterial evaluation procedure using *E. coli*.

After the designated contact time, bacteria were recovered by stirring the substrate in 5 mL of recovery solution consisting of Polysorbate 80 diluted with purified water to a concentration of 0.5%, followed by serial dilution and plating onto agar medium. The plates were incubated at 37 °C for 24 h. Antibacterial activity was quantified using the following formula:

$$\text{Bacterial density} = \frac{\text{Number of colonies} \times \text{Dilution factor}}{\text{Plating volume}}$$

Each condition was tested in triplicate, and the mean values were calculated. Error bars represent ± standard deviation. The test specimens included lactic acid-coated C1100, SUS430, and SPCC substrates (15 × 15 mm^2 each), as well as cover glass as a comparative material. Control experiments without plasma irradiation and without precursor supply were also performed.

3. Results

3.1. Effect of Precursor Delivery Method on Thin-Film Deposition

C1100 copper substrates were used to investigate the surface characteristics after film deposition with lactic acid, MCT oil, linseed oil, and citric acid-methanol mixture. Both bubbling and nebulization methods were employed for precursor supply; however, the citric acid-methanol mixture was applied only using the nebulization method.

Figure 3 shows the FT-IR spectra of C1100 substrates coated with lactic acid using bubbling and nebulization methods. For comparison, spectra of untreated samples and pure lactic acid are also presented. In plasma-treated samples, absorption bands were observed at approximately 1730 cm^{-1}, corresponding to C=O stretching vibrations of ester groups; around 1580 cm^{-1}, attributed to the asymmetric stretching of carboxylate ions (COO^-); near 1450 cm^{-1}, assigned to the symmetric stretching of carboxylate ions (COO^-) [31]; and in the range of 1200–1000 cm^{-1}, associated with C-O stretching vibrations. These peaks indicate the formation of oxygen-containing functional groups, revealing that the lactic acid-derived films contain both carboxyl and ester functionalities. Notably, the appearance of the COO^- peak suggests the generation of carboxylate structures through deprotonation of

carboxyl groups. The appearance of the COO^- band indicates the presence of deprotonated carboxylate groups; however, this feature alone does not uniquely identify a metal-lactate coordination structure. Similar spectral features may also arise from adsorbed or oxidized oxygen-containing carbon species on copper surfaces.

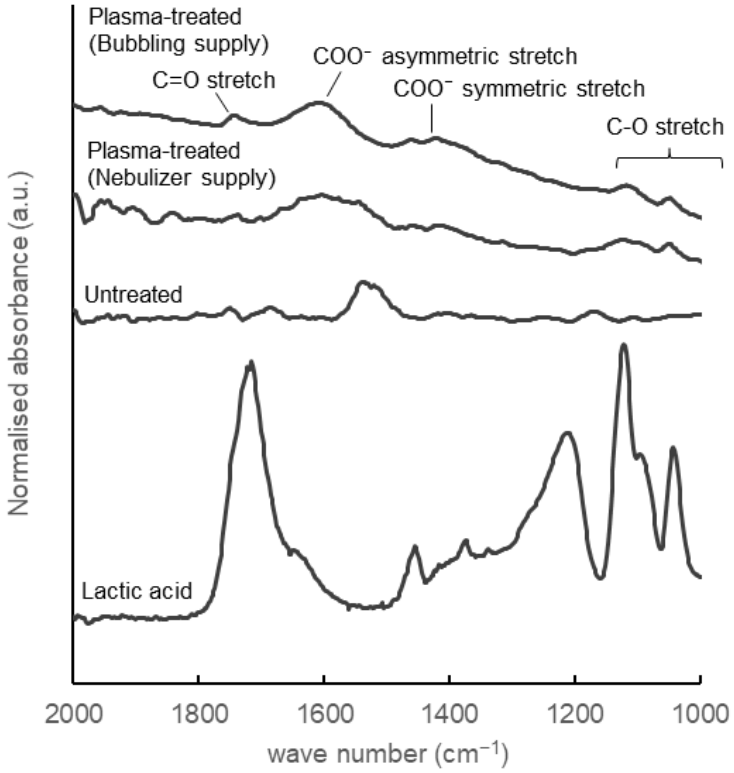


Figure 3. FT-IR spectra of C1100 copper samples after plasma treatment using lactic acid as a precursor supplied by bubbling or nebulization. Spectra were normalised to the maximum absorbance intensity and processed using a 20-point moving-average smoothing. No further spectral manipulation was applied.

To evaluate the effect of plasma discharge, Figure 4 compares the film composition with and without plasma treatment. Although argon gas was supplied in both cases, the intensity of the COO^- peak increased significantly when plasma discharge was applied, regardless of whether bubbling or nebulization was used. This result suggests that plasma discharge activates lactic acid molecules, promoting the formation of coatings containing carboxylate and ester linkages.

In contrast, for MCT oil, linseed oil, and citric acid, no significant differences were observed in FT-IR spectra between plasma-treated and untreated samples, indicating that plasma-specific film formation did not occur. Furthermore, the films obtained from MCT oil and linseed oil exhibited spectra similar to those of the original precursors, implying that the deposition was limited to simple adsorption rather than chemical bonding. This observation is supported by the supplementary FT-IR spectra of MCT oil (Figure S1), linseed oil (Figure S2), and citric acid (Figure S3), which show no substantial differences between plasma-treated and untreated samples.

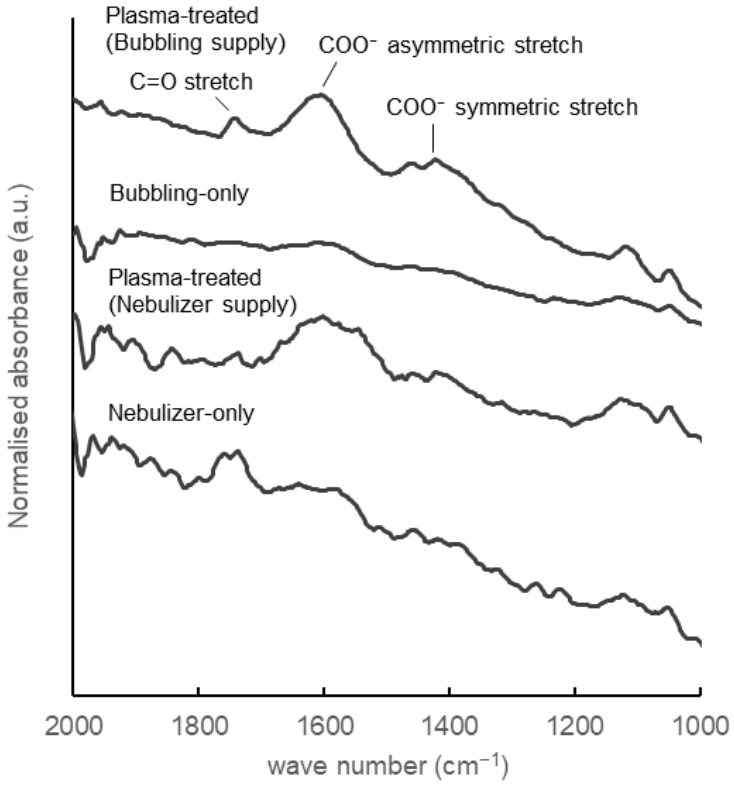


Figure 4. FT-IR spectra of C1100 copper samples coated with lactic acid under different conditions: plasma discharge with bubbling supply, bubbling-only, plasma discharge with nebulizer supply, and nebulizer-only. Spectra were normalised to the maximum absorbance intensity and processed using a 20-point moving-average smoothing. No further spectral manipulation was applied.

To perform a detailed analysis of films derived from lactic acid, the chemical bonding states were evaluated using XPS. Figure 5 shows the XPS spectra of the Cu 2p region for C1100 copper samples under different conditions: plasma treatment with bubbling supply, bubbling only, plasma treatment with nebulization supply, nebulization only, and untreated. Characteristic peaks corresponding to Cu(II), Cu(I), and Cu(0) were observed. According to literature, the Cu $2p_3/_2$ peak appears near 933 eV for Cu(II) and around 932 eV for Cu(I)/Cu(0), while Cu(II) exhibits a shake-up satellite near 942 eV [32,33]. Notably, plasma-treated samples with bubbling supply showed a distinct shake-up satellite, which is consistent with the presence of Cu(II)-like species. In contrast, plasma-treated samples with nebulization supply exhibited weaker Cu(II) peaks, with Cu(I) and Cu(0) being predominant. These findings suggest that plasma treatment combined with bubbling supply promotes the formation of Cu(II)-related features more effectively than nebulization under the present conditions.

Figure 6 presents the XPS spectra of the C 1s region for lactic acid-coated C1100 copper samples. All samples exhibited a major peak at approximately 285 eV corresponding to C-C/C-H bonds, along with peaks near 287 eV for carbonyl groups (C=O) and around 289 eV for ester groups (O-C=O) [34]. Plasma-treated samples, particularly those processed with bubbling supply, showed markedly higher intensities of C=O and O-C=O peaks compared to untreated and other treated samples, indicating that oxygen-containing functional groups derived from lactic acid were retained or introduced on the surface. In contrast, plasma treatment with nebulization supply resulted in only a limited increase, and treatments without plasma showed negligible detection of oxygen functionalities. These results demonstrate that plasma treatment combined with bubbling supply effectively

modifies surface chemistry by introducing polar functional groups, which may contribute to improved adhesion and corrosion resistance.

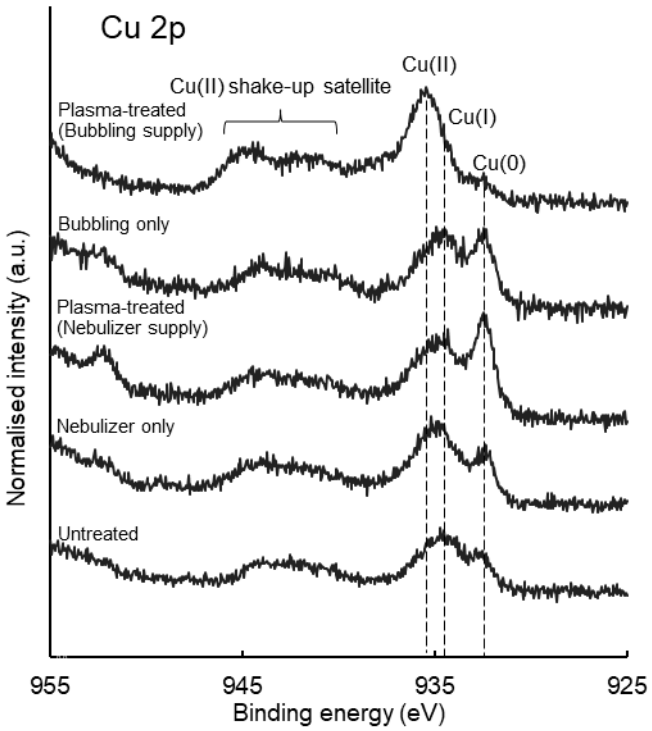


Figure 5. XPS spectra of the Cu 2p region for C1100 copper samples. Spectra were normalized to the maximum intensity of the C 1s peak to facilitate comparison of spectral shapes, and a Shirley-type background subtraction was applied. No smoothing or averaging was applied to the displayed spectra.

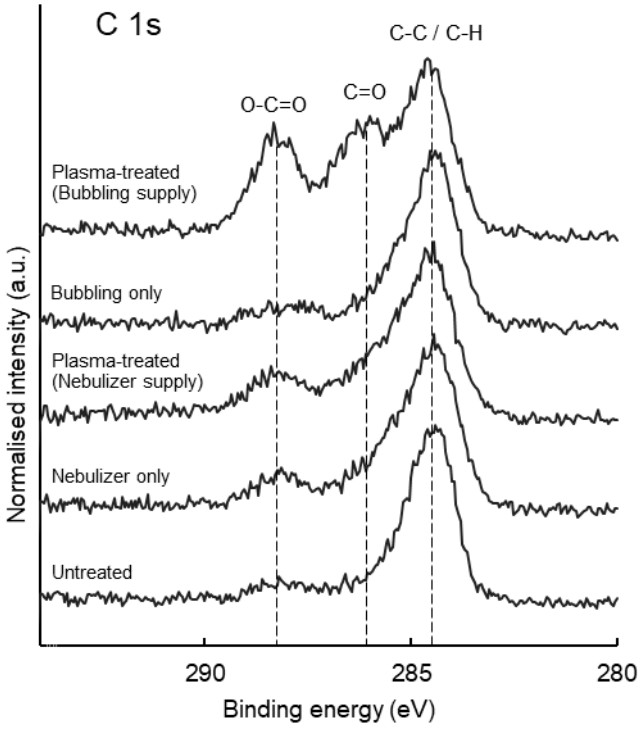


Figure 6. XPS spectra of the C 1s region for C1100 copper samples. Spectra were normalized to the maximum intensity of the C 1s peak to facilitate comparison of spectral shapes, and a Shirley-type background subtraction was applied. No smoothing or averaging was applied to the displayed spectra.

3.2. Influence of Substrate Type and Precursor Selection on Film Formation

The applicability of coating formation on SUS430 and SPCC substrates was investigated using lactic acid, MCT oil, linseed oil, and the citric acid-methanol mixture as precursors. When precursors were supplied via bubbling or nebulization at 60 °C, FT-IR spectra differing from those of the original precursors were observed only for the combination of SPCC and lactic acid under plasma discharge conditions. Figure 7 shows the FT-IR spectra of SUS430 and SPCC samples coated with lactic acid using the bubbling method. In the case of SPCC, the COO^- peak exhibited high intensity, suggesting the formation of a lactic acid-derived coating.

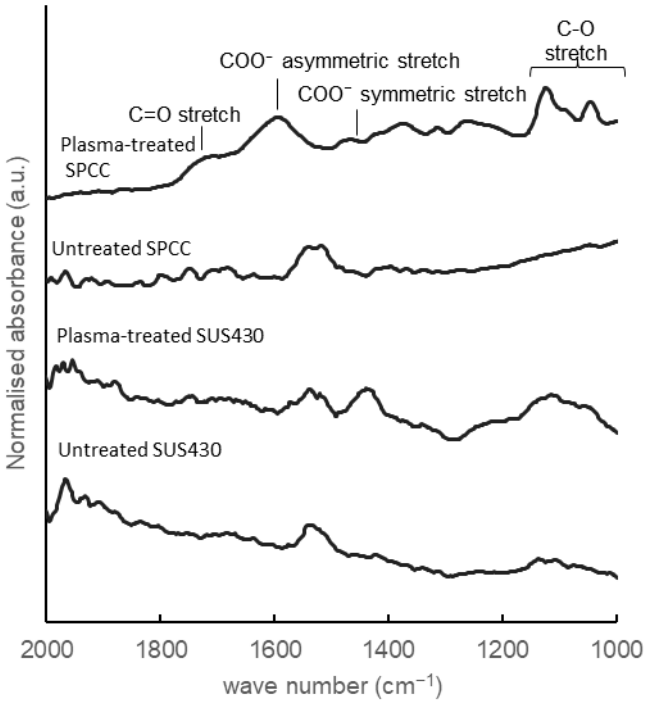


Figure 7. FT-IR spectra of SUS430 stainless steel and SPCC steel samples coated with lactic acid using plasma treatment with bubbling supply, compared with untreated samples. Spectra were normalised to the maximum absorbance intensity and processed using a 20-point moving-average smoothing. No further spectral manipulation was applied.

For antibacterial evaluation, tests were conducted on plasma-coated samples of C1100, SUS430, and SPCC prepared by supplying lactic acid through the bubbling method.

3.3. Formation Mechanism of Lactic Acid-Based Coating

Figure 8 shows the Cu 2p and C 1s spectra of C1100 copper surfaces after open-air plasma polymerization of lactic acid for different treatment times (30 s, 3 min, and 10 min), together with an untreated reference. To address film-growth-related intensity changes, the spectra in Figure 8 are plotted as counts per second (c/s), i.e., normalized by acquisition time. Therefore, within each core level, intensity trends with treatment time can be compared on a semi-quantitative basis. Cross-core-level comparisons (e.g., Cu 2p vs. C 1s) are not used quantitatively because of differences in sensitivity factors and photoionization cross sections.

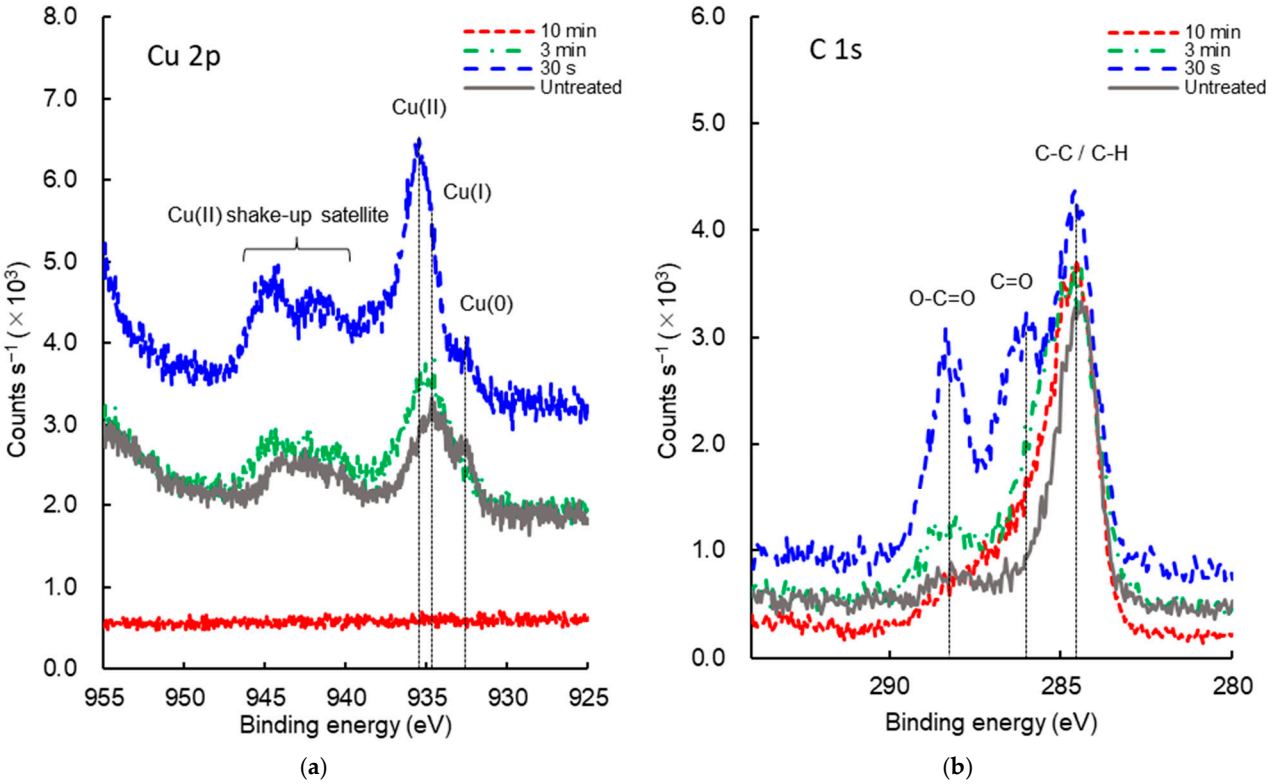


Figure 8. XPS spectra of C1100 copper surfaces coated with lactic acid by open-air plasma polymerization for different treatment times (30 s, 3 min, and 10 min), compared with an untreated sample. For clarity, the Cu 2p and C 1s spectra are displayed over 925–955 eV and 280–294 eV, respectively. The spectra are plotted on a counts-per-second (c/s) scale to retain intensity information relevant to substrate signal attenuation (i.e., no normalization to C 1s was applied in this figure). Intensities are shown as counts per second (c/s), i.e., normalized to acquisition time, and the intensity axis is scaled by 10^3 for clarity. A Shirley-type background subtraction was applied. Importantly, no smoothing or averaging was applied to the displayed spectra to avoid distortion of subtle features (e.g., shoulders/satellites in Cu 2p). (**a**) Cu 2p region; (**b**) C 1s region.

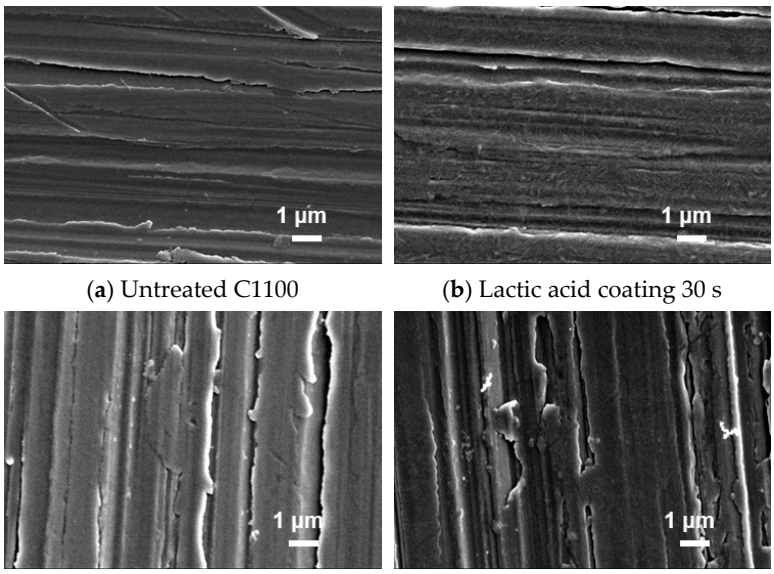
In the Cu 2p region, the 30 s sample exhibits features consistent with a Cu(II) contribution, including a shake-up satellite, during the initial stage. With increasing treatment time, the Cu 2p signal becomes progressively attenuated and approaches the noise level after 10 min, which is qualitatively consistent with increased shielding of the copper substrate by an overlayer. We note that the relatively low Cu 2p intensity of the untreated surface compared with the 30 s sample may reflect removal of adventitious surface contamination and/or changes in the native oxide during early plasma exposure.

In the C 1s region, the spectra show strong contributions near 285 eV (C-C/C-H) with additional components at higher binding energies (C=O and O-C=O), consistent with retention of oxygen-containing functionalities at short treatment times and a shift toward a more carbon-rich overlayer at longer treatment times.

To provide a quantitative basis for the time-dependent Cu 2p discussion, semi-quantitative metrics were calculated from the time-normalized spectra, including the background-subtracted integrated Cu 2p intensity (925–955 eV) and a satellite-to-main area ratio defined as Area (939–948 eV)/Area (931.5–933.0 eV) (Figure S4 and Table S1). These metrics support the observed attenuation of the Cu 2p signal with increasing treatment time, while recognizing that attenuation/information depth and lateral non-uniformity may also contribute.

SEM images in Figure 9 revealed that the untreated C1100 surface was largely featureless apart from a micrometer- to sub-micrometer-scale scratch pattern originating from the

manufacturing/polishing process. After 30 s of plasma treatment, a very fine, fuzzy texture became visible on top of the pre-existing scratches. For samples treated for 3 min and 10 min, no further distinct morphological changes were observed at the present magnification; the scratch pattern remained visible, and the surface appearance was consistent with the formation of a thin layer with uniform morphology rather than a levelling/scratch-filling effect. These results demonstrate that short treatment times produce layers rich in oxygen functional groups, while prolonged treatment leads to the growth of thick carbon-based layers that completely shield signals from the C1100 substrate. However, the magnification of the available SEM images is limited, and therefore, the observed morphological differences should be interpreted as qualitative trends rather than definitive nanoscale structural information. Higher-resolution SEM or AFM will be required in future work to clarify the detailed growth morphology of the deposited films.



(**a**) Untreated C1100 (**b**) Lactic acid coating 30 s

(**c**) Lactic acid coating 3 min (**d**) Lactic acid coating 10 min

Figure 9. SEM images of C1100 copper surfaces after lactic acid coating using an open-air plasma polymerization process for different treatment times: (**a**) untreated, (**b**) 30 s, (**c**) 3 min, and (**d**) 10 min. Images were cropped to remove unused margins, and only uniform brightness/contrast adjustments were applied. No smoothing, filtering, or additional image processing was performed. A scratch pattern originating from the manufacturing/polishing process is visible in all images; the 30 s sample additionally shows a faint fuzzy texture superimposed on the scratches.

3.4. Substrate-Dependent Antibacterial Responses of Lactic-Acid-Treated Surfaces

Because this study primarily focuses on interface chemistry and film formation, the antibacterial test is presented here as a secondary functional check rather than a central performance claim. It should be emphasized that this antibacterial evaluation was conducted to determine whether any coating-attributable antibacterial effect could be distinguished from substrate-driven or transient effects. Figure 10 presents the antibacterial evaluation results for samples coated with lactic acid on C1100, SUS430, and SPCC substrates. For C1100 (copper), the bacterial count remained below the detection limit regardless of coating, indicating that the strong intrinsic antibacterial activity of copper dominated the response, with no additional effect attributable to the lactic-acid-derived film. In the case of SUS430, no significant difference was observed between coated and uncoated samples. Combined with the absence of characteristic FT-IR peaks, this indicates that the lactic-acid-derived film did not form on the passive stainless-steel surface and therefore did not impart antibacterial activity. In contrast, for SPCC, the bacterial count temporarily dropped below the detection

limit at 2 h on the coated surface; however, this effect disappeared at 6 h and 24 h. This transient reduction is attributed to substrate-acid reactions—such as local acidification and iron lactate formation—rather than an intrinsic antibacterial property of the plasma polymer film.

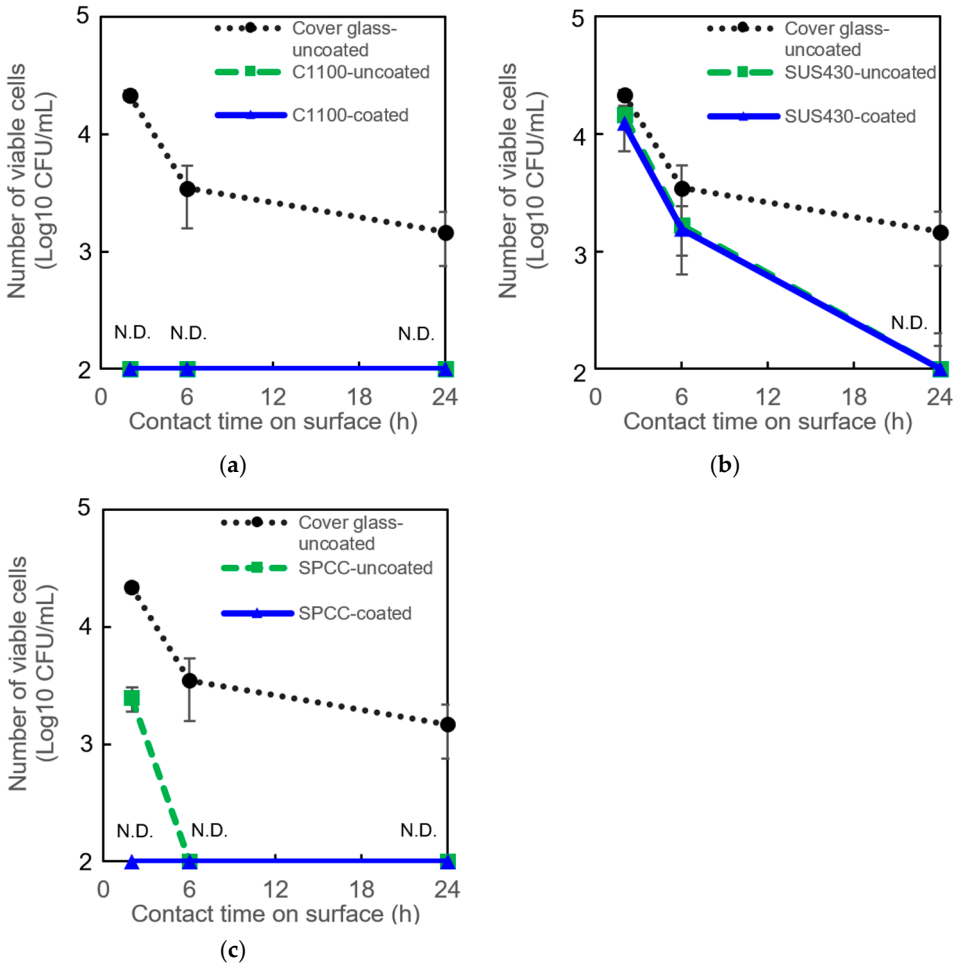


Figure 10. Antibacterial test results (secondary functional check) for lactic acid-treated samples on different substrates evaluated by viable cell counts (CFU mL^{-1}) as a function of contact time on the surface: (**a**) C1100 copper, (**b**) SUS430 stainless steel, and (**c**) SPCC steel. N.D. indicates that the bacterial count was below the detection limit (10^2 CFU mL^{-1}).

4. Discussion

Scope and limitations. The present work focuses on comparative surface-chemistry trends and deposition behavior under open-air plasma polymerization, supported by FT-IR, XPS, and surface SEM. While these data suggest the formation of an interfacial metal-lactate-like region and an overlayer, the interface is not directly imaged here; therefore, the interfacial model is presented as a qualitative interpretation rather than a definitive structural determination. To strengthen the time-dependent XPS discussion, we additionally provide semi-quantitative Cu 2p metrics derived from the time-normalized spectra (Figure S4 and Table S1), while recognizing that attenuation/information depth and lateral non-uniformity remain plausible contributors.

This study elucidates the formation mechanism of lactic-acid-derived films produced by open-air plasma polymerization and clarifies how precursor delivery methods and plasma conditions influence film deposition. Rather than demonstrating an intrinsic antibac-

terial function of the coatings, the results reveal that both film formation and antibacterial behavior are strongly substrate-dependent.

For lactic-acid-based coatings, film formation was successfully achieved on both C1100 copper and SPCC steel substrates using bubbling and nebulization. FT-IR and XPS analyses showed that, on C1100 copper, the bubbling method produced pronounced signals corresponding to carboxyl groups and Cu(II), which is consistent with the possible presence of copper(II)-carboxylate-like interfacial species [35–38]. However, the XPS data do not provide direct evidence for a specific copper-lactate coordination structure, and the observed Cu(II) and oxygenated carbon signals may also originate from surface oxidation, hydroxylation, or non-specific adsorption of oxygen-containing carbon species. Plasma irradiation combined with bubbling further enhanced the generation of copper(II) lactate and increased carbonyl-group intensity, indicating strong interfacial bonding. In contrast, nebulization likely resulted in surface adsorption of undecomposed precursor molecules due to the high supply rate. Because copper(II) lactate is expected to localize mainly at the interface, it may remain undetected by XPS due to the limited analysis depth [39]. Optimization of spray amount and droplet size will be necessary to improve film uniformity and chemical-bond formation when using nebulization.

The conclusion that nebulization primarily leads to adsorption, whereas bubbling with plasma irradiation yields film formation, is based on differences in XPS intensities and the appearance of plasma-specific COO^-/C=O bands in FT-IR spectra. Although these trends strongly indicate distinct deposition mechanisms, the current data are insufficient to decisively differentiate adsorption from plasma-polymer-type growth. Additional evidence—such as quantitative mass uptake, adhesion assessments, water-washing stability, and thickness measurements—will be required to validate the proposed mechanism. These studies are planned for future work. It should also be noted that the COO^--related FT-IR peaks observed on C1100 may not originate solely from plasma-induced reactions. Previous studies have shown that lactic acid can form Cu(II) lactate even without plasma, producing carboxylate-related peaks in similar spectral regions [40]. Therefore, the COO^- signals identified here likely include contributions from substrate-driven interfacial reactions. Although plasma irradiation increased the COO^- peak intensity—implying an additional activation pathway—further analysis is required to distinguish plasma-induced contributions from those arising from copper-lactic acid chemistry. Future work will incorporate experiments using inert substrates and time-resolved surface analyses.

For SUS430 and SPCC substrates, lactic-acid-based coatings were confirmed only on SPCC under bubbling conditions. This likely reflects the formation of iron lactate, which promotes initial bonding on SPCC [41,42]. In contrast, SUS430 showed no coating formation, presumably due to inhibition by its passive chromium-oxide layer. For MCT oil, linseed oil, and citric acid, no differences were observed in the FT-IR spectra with or without plasma irradiation, indicating that the plasma-assisted effect was not evident under the present conditions.

The selective film formation observed for lactic acid can be rationalized by comparing the physicochemical properties of the precursors. First, lactic acid has significantly higher volatility at 60 °C (Table 1), providing a molecular flux several orders of magnitude larger than that of MCT and linseed oils, thereby increasing the likelihood of plasma activation. Second, lactic acid possesses a high density of reactive functional groups (one carboxyl and one hydroxyl), which readily undergo plasma-induced fragmentation and recombination to form carbonyl- and COO^--containing species. In contrast, MCT and linseed oils consist mainly of long-chain triglycerides with low functional-group density, leading primarily to physisorbed films with minimal plasma-specific modification (Supplementary Figures S1 and S2). Third, as an α-hydroxy acid, lactic acid can chelate Cu^{2+}, stabilizing

surface-bound intermediates and promoting Cu-O-C bond formation. Such behavior is absent in triglycerides and weak in citric acid under nebulized methanol delivery. These combined factors explain why lactic acid uniquely supports plasma-driven polymer-like film formation.

On C1100 substrates, lactic acid coatings formed under plasma irradiation showed an increase in carboxyl groups, C=O, and Cu(II) after 30 s of treatment. However, with longer treatment times, C-C/C-H peaks became dominant, and copper-related signals diminished. After 10 min, copper signals disappeared completely, suggesting substantial attenuation of the copper signal, which is consistent with a tentative model involving an oxygen-rich interfacial region that may include metal-carboxylate-like bonding, followed by the accumulation of a carbon-rich overlayer. These findings suggest that plasma irradiation induces hydrogen abstraction from lactic acid carboxyl groups, generating radical species that form complexes with copper atoms. However, this interpretation remains qualitative, as the present data do not allow discrimination between specific metal-lactate species and more generic oxygenated carbon layers. During film growth, decomposition products lacking carboxyl groups likely contributed to the formation of a carbon-rich layer dominated by C-C and C-H bonds. Lactic acid decomposition products (acetaldehyde, CO_2, CO, H_2O) [24,43] may have been radicalized in the plasma but did not remain stable on the substrate; instead, they were incorporated into the film as carbon frameworks. SEM observations revealed fine surface features after 30 s of treatment, whereas samples treated for 3 min or longer exhibited uniform surfaces. It should be noted that this bilayer structure is a proposed model derived from spectroscopic tendencies rather than a directly observed structure. The schematic aims to rationalize the observed COO^- enrichment at the interface and the carbon-rich overlayer indicated by XPS. Overall, the spectroscopic trends are consistent with a conceptual bilayer-like model comprising a metal-lactate-like interfacial region and a carbon-rich overlayer (Figure 11), while attenuation effects and laterally heterogeneous coverage cannot be excluded without quantitative thickness/coverage measurements.

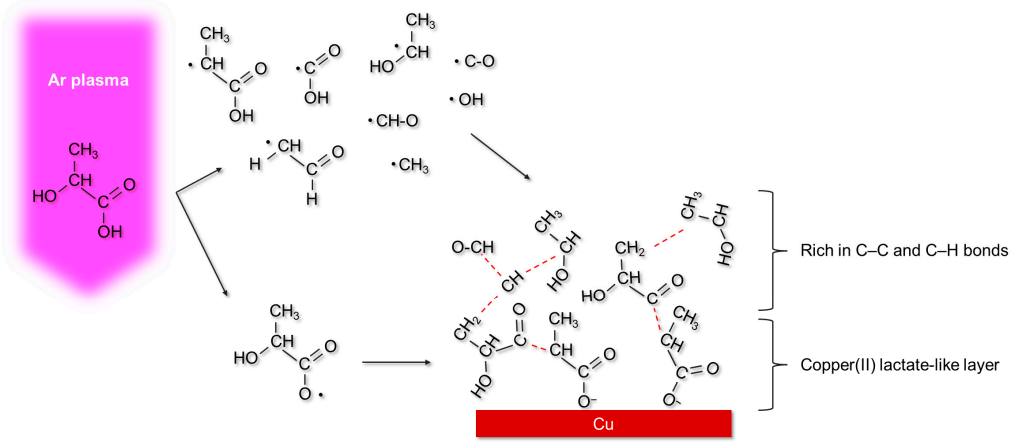


Figure 11. Proposed schematic model illustrating one possible interpretation of the observed spectroscopic trends for lactic-acid-derived coatings on copper. This schematic does not represent a definitive structural identification of the interface. The assignment of metal-lactate-like bonding is tentative, and alternative explanations such as adsorption, oxidation, or generic oxygenated carbon deposition cannot be excluded based on the present data.

Quantitative film thickness measurement, such as spectroscopic ellipsometry, could not be performed. Consequently, the discussion in this work is restricted to qualitative trends inferred from FT-IR, XPS, and low-magnification SEM observations. Future studies will include ellipsometry, profilometry, or cross-sectional SEM to quantitatively determine film thickness and correlate it with deposition conditions.

Although FT-IR and XPS analyses revealed plasma-induced formation of carbonyl- and carboxylate-containing species, the present data are not sufficient to conclusively demonstrate that the deposited layer constitutes a solid plasma-polymerized thin film rather than an adsorbed oily layer. Direct evidence such as film hardness, quantitative thickness determination, depth-resolved compositional profiling (e.g., GD-OES), and solubility or water-washing stability tests will be required to verify the presence of a solid, cross-linked thin film. These analyses will be included in future work.

Furthermore, while the chemical signatures observed in this study are consistent with random, highly cross-linked networks typically formed during plasma polymerization, the results do not fully prove that the obtained films are plasma-polymerized random polymers derived from lactic acid. Definitive structural verification would require additional analyses such as mass spectrometry, NMR-based reconstruction of fragmentation pathways, or detailed depth-resolved chemical mapping. Incorporating these advanced characterizations represents an important direction for future investigation.

Antibacterial testing was included as a secondary functional check to assess whether any coating-attributable effect could be separated from substrate-driven responses. The outcomes were substrate-dominated and/or transient (Figure 10), indicating that the deposited layer under the present conditions does not provide a robust antibacterial function. This functional check therefore supports the main conclusion that interface chemistry and film formation (or lack thereof) govern the observed surface responses.

5. Conclusions

In this study, lactic-acid-derived films were successfully deposited using an open-air plasma polymerization process, and the plasma-assisted mechanisms of film formation were elucidated. Film deposition was achieved with both nebulization and bubbling precursor-delivery methods; however, FT-IR and XPS analyses revealed that the bubbling method promoted more pronounced chemical bonding, the bubbling method promoted more pronounced plasma-assisted interfacial chemistry, possibly involving metal-carboxylate-like interactions. However, the present study does not provide direct, discriminating evidence for a specific copper-lactate interfacial species, and the proposed interfacial model should be regarded as a tentative interpretation rather than a definitive structural identification.

The influence of treatment time showed a clear evolution from oxygen-rich functional layers at short exposure times to carbon-rich films at longer exposures, during which copper signals became strongly attenuated and eventually fell below the detection limit. Combined spectroscopic and microscopic analyses suggest that lactic acid undergoes plasma-induced fragmentation and recombination, consistent with a conceptual model involving a metal-lactate-like interfacial region and a carbon-rich overlayer, although alternative interpretations related to attenuation and non-uniform coverage remain possible.

Overall, this study elucidates the plasma-assisted formation mechanism and interfacial chemistry of lactic-acid-derived films under open-air conditions. As a secondary functional check, antibacterial testing showed substrate-dominated and/or transient responses (Figure 10), providing a boundary condition for future design of coating-attributable antibacterial functionality.

Supplementary Materials: The following supporting information can be downloaded at: https://www.mdpi.com/article/10.3390/surfaces9020033/s1, Figure S1: Normalised ATR-FT-IR spectra of plasma-treated (bubbling supply), plasma-treated (nebulizer supply), untreated copper, and MCT oil reference in the 2000–1000 cm^{-1} region; Figure S2: Normalised ATR-FT-IR spectra of plasma-treated (bubbling supply), plasma-treated (nebulizer supply), untreated copper, and linseed oil reference in the 2000–1000 cm^{-1} region; Figure S3: Normalised ATR-FT-IR spectra of plasma-treated (nebulizer

supply), nebulizer-only, untreated copper, and citric acid reference in the 2000–1000 cm^{-1} region; Figure S4: Semi-quantitative time dependence of Cu 2p metrics derived from time-normalized (c/s) spectra, including (a) integrated Cu 2p intensity (925–955 eV) and (b) satellite-to-main area ratio defined as Area (939–948 eV)/Area (931.5–933.0 eV), calculated after Shirley background subtraction; Table S1: Semi-quantitative Cu 2p areas and satellite-to-main ratios used for Figure S4 (Shirley-subtracted, time-normalized spectra).

Author Contributions: Conceptualization, A.O. and S.Y.; methodology, S.Y., T.O. and M.T.; investigation, S.Y., A.S., H.-T.H. and T.F.; writing—original draft preparation, S.Y.; writing—review and editing, S.Y., A.O. and A.Y.; project administration, A.O. All authors have read and agreed to the published version of the manuscript.

Funding: This research was funded by JSPS, grant number (S) 22H04973.

Institutional Review Board Statement: Not applicable.

Informed Consent Statement: Not applicable.

Data Availability Statement: The raw data supporting the conclusions of this article will be made available by the authors on request.

Conflicts of Interest: The authors declare no conflicts of interest. One of the authors is employed by a company; however, the company had no role in the design of the study; in the collection, analyses, or interpretation of data; in the writing of the manuscript; or in the decision to publish the results. The funders had no role in the design of the study; in the collection, analyses, or interpretation of data; in the writing of the manuscript; or in the decision to publish the results.

Abbreviations

The following abbreviations are used in this manuscript:

DBD	Dielectric Barrier Discharge
MCT	Medium-Chain Triglyceride
SPCC	Steel Plate Cold Commercial

References

1. Encinas, N.; Dillingham, R.G.; Oakley, B.R.; Abenojar, J.; Martínez, M.A.; Pantoja, M. Adhesion Enhancement by Closed-System Plasma Treatment. *J. Adhes.* **2012**, *88*, 321–336. [CrossRef]
2. Kikuchi, T.; Bai, L.; Mitarai, T.; Yagi, H.; Furukawa, M.; Amemiya, T.; Nishiyama, N.; Arai, S. Bonding Improvement Using Closed-System Plasma Treatment. *Jpn. J. Appl. Phys.* **2020**, *59*, SBBD02. [CrossRef]
3. Tendero, C.; Tixier, C.; Tristant, P.; Desmaison, J.; Leprince, P. Atmospheric Pressure Plasmas: A Review. *Spectrochim. Acta Part B* **2006**, *61*, 2–30. [CrossRef]
4. Yanagawa, Y.; Suenaga, Y.; Iijima, Y.; Endo, M.; Sanada, N.; Katoh, E.; Toki, S.; Okino, A.; Mitsuhara, I. Temperature-controlled atmospheric-pressure plasma treatment induces protein uptake via clathrin-mediated endocytosis in tobacco cells. *Plant Biotechnol.* **2022**, *39*, 179–183. [CrossRef]
5. Yanagawa, Y.; Kawano, H.; Kobayashi, T.; Miyahara, H.; Okino, A.; Mitsuhara, I. Direct protein introduction into plant cells using a multi-gas plasma jet. *PLoS ONE* **2017**, *12*, e0171942. [CrossRef]
6. Turkoglu Sasmazel, H.; Alazzawi, M.; Kadim Abid Alsahib, N. Atmospheric Pressure Plasma Surface Treatment of Polymers and Influence on Cell Cultivation. *Molecules* **2021**, *26*, 1665. [CrossRef] [PubMed]
7. Ahmed, M.W.; Gul, K.; Mumtaz, S. Recent Advances in Cold Atmospheric Pressure Plasma for *E. coli* Decontamination in Food: A Review. *Plasma* **2025**, *8*, 18. [CrossRef]
8. Laroussi, M. Cold Plasma in Medicine and Healthcare: The New Frontier in Low Temperature Plasma Applications. *Front. Phys.* **2020**, *8*, 74. [CrossRef]
9. Takamatsu, T.; Hirai, H.; Sasaki, R.; Miyahara, H.; Okino, A. Surface Hydrophilization of Polyimide Films Using Atmospheric Damage-Free Multigas Plasma Jet Source. *IEEE Trans. Plasma Sci.* **2013**, *41*, 119–125. [CrossRef]
10. Lopez, E.; Dresler, B.; Mäder, G.; Dani, I.; Hopfe, V.; Kaskel, S.; Heintze, M.; Möller, R.; Wanka, H.; Kirschmann, M.; et al. Advanced Coating Technologies for Vacuum Applications. *Proc. Soc. Vac. Coaters* **2008**, *51*, 622–626.

11. Furuya, J.; Hihara, K.; Fukuchi, K.; Osawa, T.; Yaida, A.; Okino, A. Atmospheric Linear-Type Mixed-Gas Plasma Source with Low-Particle Emission for Large Area Surface Treatment. *Int. J. Plasma Environ. Sci. Technol.* **2025**, *19*, e02025.
12. Yoshida, S.; Hihara, K.; Furuya, J.; Osawa, T.; Yaida, A.; Nishiyama, N.; Okino, A. Development of a Low-Particle Emission Linear Atmospheric Plasma Device for Hydrophilization of Silicon Wafers. *Appl. Sci.* **2025**, *15*, 10349. [CrossRef]
13. Đurđević-Milošević, D.; Petrović, A.; Kalaba, V.; Stijepić, M.; Jovanović, G. Selected Aspects of the Antibacterial Use of Lactic Acid in Food Processing. *Eng. Proc.* **2024**, *67*, 2.
14. Koiso, H. Food additives to control microorganisms: Mechanisms and current status. *Jpn. J. Food Microbiol.* **2014**, *31*, 70–75. [CrossRef]
15. Dongare, A.; Shivasharan, U.; Hosmani, A.H. Antimicrobial Activity of Flaxseed Marketed Oil on Different Microbes. *Int. J. Sci. Res. Sci. Technol.* **2023**, *10*, 21–25.
16. Alyami, H.R.; Wu, Y.; Aljughaiman, A.; Li, T.; Almulhim, A.; Bliss, J.M.; Xiao, J. The Effect of Medium-Chain Triglycerides Oil on Candida albicans and Streptococcus mutans in Planktonic and Mucosal Models. *Antibiotics* **2024**, *13*, 1231. [CrossRef]
17. Aromaa, J.; Kekkonen, M.; Mousapour, M.; Jokilaakso, A.; Lundström, M. The Oxidation of Copper in Air at Temperatures up to 100 °C. *Corros. Mater. Degrad.* **2021**, *2*, 625–640. [CrossRef]
18. Roy, S.K.; Ananth, V.; Bose, S.K. Oxidation Behavior of Copper at High Temperatures under Two Different Modes of Direct-Current Applications. *Oxid. Met.* **1995**, *43*, 185–215. [CrossRef]
19. Haapakangas, J.; Riikonen, S.; Airaksinen, S.; Heikkinen, E.-P.; Fabritius, T. Oxide Scale Formation on Low-Carbon Steels in Future Reheating Conditions. *Metals* **2024**, *14*, 189. [CrossRef]
20. Wang, R.; Ohgata, Y.; Li, Y.; Xiao, T.; Honda, M. Tribocorrosion behaviour of SUS430 stainless steel in aqueous solutions with different pH. *Coatings* **2023**, *13*, 1539. [CrossRef]
21. Grass, G.; Rensing, C.; Solioz, M. Metallic Copper as an Antimicrobial Surface. *Appl. Environ. Microbiol.* **2011**, *77*, 1541–1547. [CrossRef]
22. Warnes, S.L.; Keevil, C.W. Mechanism of copper surface toxicity in *Escherichia coli* O157:H7 and Salmonella involves immediate membrane depolarization followed by slower rate of DNA destruction which differs from that observed for Gram-positive bacteria. *Environ. Microbiol.* **2011**, *13*, 2389–2397. [CrossRef]
23. Emel'yanenko, V.N.; Verevkin, S.P.; Schick, C. The thermodynamic properties of S-lactic acid. *Russ. J. Phys. Chem. A* **2010**, *84*, 1491–1497. [CrossRef]
24. Komesu, A.; Martinez, P.F.M.; Lunelli, B.H.; Oliveira, J.; Maciel, M.R.W.; Maciel Filho, R. Study of lactic acid thermal behavior using thermoanalytical techniques. *J. Chem.* **2017**, *2017*, 4149592. [CrossRef]
25. Wilson, J.A.; Chickos, J.S. Vapor pressures and vaporization, sublimation, and fusion enthalpies of some fatty acids. *J. Chem. Eng. Data* **2013**, *58*, 322–333. [CrossRef]
26. Verevkin, S.P.; Nagrimanov, R.N. Non-Covalent Interactions in Triglycerides: Vaporisation Thermodynamics for Quantification of Dispersion Forces. *Thermo* **2022**, *2*, 250–266. [CrossRef]
27. Acree, W.E., Jr.; Chickos, J.S. Phase Transition Enthalpy Measurements of Organic and Organometallic Compounds. Sublimation, Vaporization and Fusion Enthalpies From 1880 to 2015. Part 1. C_1–C_{10}. *J. Phys. Chem. Ref. Data* **2016**, *45*, 033101. [CrossRef]
28. *ISO 22196*; Measurement of Antibacterial Activity on Plastics and Other Non-Porous Surfaces. International Organization for Standardization: Geneva, Switzerland, 2011.
29. Michels, H.T.; Anderson, D.G. Antimicrobial Regulatory Efficacy Testing of Solid Copper Alloy Surfaces in the USA. *Met. Ions Biol. Med.* **2008**, *10*, 185–190.
30. Kaur, H.; Rosenberg, M.; Kook, M.; Danilian, D.; Kisand, V.; Ivask, A. Antibacterial Activity of Solid Surfaces Is Critically Dependent on Relative Humidity, Inoculum Volume, and Organic Soiling. *FEMS Microbes* **2024**, *5*, xtad022. [CrossRef]
31. Silverstein, R.M.; Webster, F.X. *Spectrometric Identification of Organic Compounds*, 6th ed.; Wiley: New York, NY, USA, 1998; pp. 1–495.
32. Kawasaki, S. Satellite Peaks in XPS Spectra. *J. Surf. Anal.* **2024**, *31*, 120–136. [CrossRef]
33. Biesinger, M.C. Advanced analysis of copper X-ray photoelectron spectra. *Surf. Interface Anal.* **2017**, *49*, 1325–1334. [CrossRef]
34. Grey, L.H.; Nie, H.-Y.; Biesinger, M.C. Defining the nature of adventitious carbon and improving its merit as a charge correction reference for XPS. *Appl. Surf. Sci.* **2024**, *653*, 159319. [CrossRef]
35. Nishioka, K.; Okada, M.; Kanzaki, R.; Fukami, K.; Murase, K. Copper(II)-Lactate Complexes in Cu_2O Electrodeposition Baths: Stability of the Complexes and Aging of the Baths. *J. Electrochem. Soc.* **2025**, *172*, 032511. [CrossRef]
36. Chen, T.; Kitada, A.; Seki, Y.; Fukami, K.; Usmanov, D.T.; Chen, L.C.; Hiraoka, K.; Murase, K. Identification of Copper(II)-Lactate Complexes in Cu_2O Electrodeposition Baths: Deprotonation of the α-Hydroxyl Group in Highly Concentrated Alkaline Solution. *J. Electrochem. Soc.* **2018**, *165*, D444–D451. [CrossRef]
37. Deng, J.; Wen, S.; Deng, J.; Wu, D.; Yang, J. Extracting Copper by Lactic Acid from Copper Oxide Ore and Dissolution Kinetics. *J. Chem. Eng. Jpn.* **2015**, *48*, 538–544. [CrossRef]

38. Fujiwara, M.; Matsushita, T.; Ikeda, S. X-Ray Photoelectron Spectroscopy of Copper(II) Complexes with Donor Sets of O_4, N_2O_4, N_2O_2, N_4, N_2S_2, and S_4. *Anal. Sci.* **1993**, *9*, 289–291. [CrossRef]
39. Tanuma, S.; Powell, C.J.; Penn, D.R. Calculations of electron inelastic mean free paths. IX. Data for 41 elemental solids over the 50 eV to 30 keV range. *Surf. Interface Anal.* **2011**, *43*, 689–713. [CrossRef]
40. Wang, X.; Zhang, Z.; Feng, Y.; Xiao, F. Anti-oxidative copper nanoparticle paste for Cu-Cu bonding at low temperature in air. *J. Mater. Sci. Mater. Electron.* **2022**, *33*, 817–827. [CrossRef]
41. Pozdnyakov, I.P.; Wu, F.; Melnikov, A.A.; Grivin, V.P.; Bazhin, N.M.; Chekalin, S.V.; Plyusnin, V.F. Photochemistry of iron(III)-lactic acid complex in aqueous solutions. *Russ. Chem. Bull. Int. Ed.* **2013**, *62*, 1579–1585. [CrossRef]
42. Yamada, A. Polarographic Studies of Fe(III) Lactate Complex Ions. *Nippon Kagaku Zasshi* **1963**, *84*, 709–719. [CrossRef]
43. Zhu, S.; Kumagai, S.; Kimeda, T.; Sato, Y.; Yoshioka, T. Effects of heating rate and temperature on product distribution of poly-lactic acid and poly-3-hydroxybutyrate-co-3-hydroxyhexanoate. *J. Mater. Cycles Waste Manag.* **2023**, *25*, 650–661.

Disclaimer/Publisher's Note: The statements, opinions and data contained in all publications are solely those of the individual author(s) and contributor(s) and not of MDPI and/or the editor(s). MDPI and/or the editor(s) disclaim responsibility for any injury to people or property resulting from any ideas, methods, instructions or products referred to in the content.